

---

# Pose-RFT: Enhancing MLLMs for 3D Pose Generation via Hybrid Action Reinforcement Fine-Tuning

---

**Bao Li<sup>1,2</sup> Xiaomei Zhang<sup>1,2</sup> Miao Xu<sup>1,3</sup> Zhaoxin Fan<sup>4</sup> Xiangyu Zhu<sup>1,2</sup> Zhen Lei<sup>1,2,3</sup>**

<sup>1</sup>CASIA <sup>2</sup>UCAS <sup>3</sup>CAIR, HKISI, CAS <sup>4</sup>Beihang University

{libao2023, zhangxiaomei2016, xiangyu.zhu, zhen.lei}@ia.ac.cn

miao.xu@cair-cas.org.hk zhaoxinf@buaa.edu.cn

## Abstract

Generating 3D human poses from multimodal inputs such as images or text requires models to capture both rich spatial and semantic correspondences. While pose-specific multimodal large language models (MLLMs) have shown promise in this task, they are typically trained with supervised objectives such as SMPL parameter regression or token-level prediction, which struggle to model the inherent ambiguity and achieve task-specific alignment required for accurate 3D pose generation. To address these limitations, we propose Pose-RFT, a reinforcement fine-tuning framework tailored for 3D human pose generation in MLLMs. We formulate the task as a hybrid action reinforcement learning problem that jointly optimizes discrete language prediction and continuous pose generation. To this end, we introduce HyGRPO, a hybrid reinforcement learning algorithm that performs group-wise reward normalization over sampled responses to guide joint optimization of discrete and continuous actions. Pose-RFT further incorporates task-specific reward functions to guide optimization towards spatial alignment in image-to-pose generation and semantic consistency in text-to-pose generation. Extensive experiments on multiple pose generation benchmarks demonstrate that Pose-RFT significantly improves performance over existing pose-specific MLLMs, validating the effectiveness of hybrid action reinforcement fine-tuning for 3D pose generation.

## 1 Introduction

Recent advances in 3D human pose generation [10, 11, 18, 44] have increasingly focused on addressing the problem of understanding and reasoning about 3D human poses from multimodal inputs, such as images and text. Among these, pose-specific multimodal large language models (MLLMs) [14, 27] have emerged as a promising direction, extending general-purpose language models with dedicated pose decoders to enable joint reasoning over language, vision, and 3D pose. These models have shown strong performance across both image-to-pose and text-to-pose generation tasks.

Despite their progress, current pose-specific MLLMs are typically trained with supervised objectives such as SMPL [33] parameter regression [14] or token-level prediction [27]. While these objectives enforce consistency with annotated data, they are insufficient for capturing the inherent ambiguity and the task-specific spatial and semantic alignment required in 3D pose generation. In image-to-pose generation, ambiguity arises from depth and perspective limitations in 2D images, which often correspond to multiple plausible 3D poses. For text-to-pose generation, the challenge is further compounded by the vagueness and subjectivity of natural language, which results in a broad distribution over valid poses. As illustrated in Fig. 1, distinct 3D poses may yield similar reconstruction losses (e.g., MSE) despite exhibiting clear semantic differences. This highlights the limitations of standard supervised objectives and motivates the need for reward signals that better reflect semantic alignment.

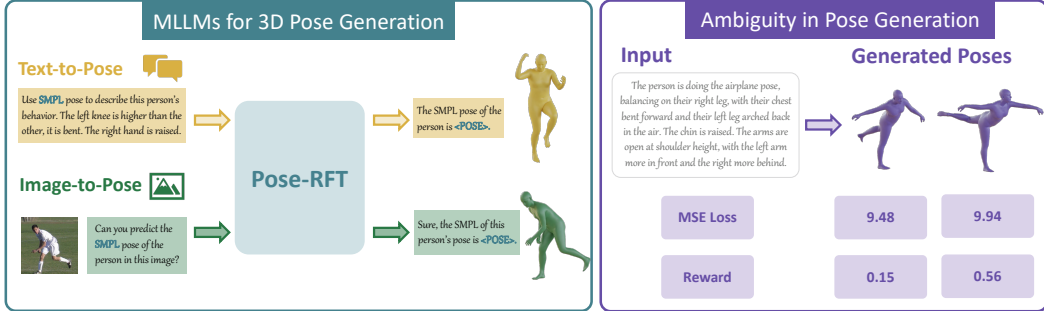


Figure 1: **Examples and Motivation.** **Left:** Our proposed Pose-RFT, an enhanced multimodal large language model, generates 3D SMPL human pose given either text or image input. **Right:** Two 3D poses generated from the same prompt yield comparable MSE loss, while the reward reflects their difference in semantic alignment.

These challenges motivate the use of reinforcement learning (RL), which provides a principled approach for optimizing models beyond supervised labels, toward more aligned spatial and semantic outputs. However, most existing reinforcement fine-tuning (RFT) algorithms [1, 21, 32, 42, 26] operate in purely discrete token spaces and are primarily designed for language-level alignment. Such discrete approaches are inherently limited for optimizing the fine-grained, continuous outputs required in 3D human pose generation.

To address these challenges, we propose Pose-RFT (see Fig. 2), a reinforcement fine-tuning framework specifically designed for 3D human pose generation in MLLMs. **First**, we formulate the task as a hybrid action space reinforcement learning problem, where the policy simultaneously produces discrete actions (e.g., text tokens) and continuous actions (e.g., 3D pose parameters). Inspired by prior work in hybrid RL [34, 13, 25], we construct a unified representation space leveraging the language-aligned multimodal embeddings of existing pose-specific MLLMs. The continuous action is modeled by a multivariate Gaussian policy, parameterized by a pose head that outputs both the mean and covariance. **Second**, we introduce HyGRPO, an online hybrid reinforcement learning algorithm built upon GRPO [41], which directly optimizes policies over the original hybrid action space. For each input, the pretrained pose-specific MLLM generates multiple hybrid responses (text + pose), normalizes the reward scores within the group, and updates the policy to prefer responses with higher rewards. **Third**, we propose four verifiable, task-specific reward functions to guide policy optimization: (i) a spatial location reward for image-to-pose generation, (ii) a semantic alignment reward for text-to-pose generation, (iii) a format correctness reward, and (iv) a text embedding similarity reward. By training with diverse outputs and structured feedback, HyGRPO encourages the model to generate 3D poses that are spatially accurate and semantically aligned.

In summary, our main contributions are as follows:

(1) We propose Pose-RFT, the first reinforcement fine-tuning framework specifically designed for 3D human pose generation in MLLMs. (2) We develop HyGRPO, a hybrid-action reinforcement learning algorithm that effectively optimizes both discrete and continuous outputs in pose-specific MLLMs. (3) Extensive experiments on multiple pose generation benchmarks demonstrate that Pose-RFT significantly improves performance over existing pose-specific MLLMs, validating the effectiveness of hybrid action reinforcement fine-tuning for 3D pose generation.

## 2 Related Work

### 2.1 Human Pose Generation

Human pose generation involves producing 3D human poses conditioned on either images or text. For image-to-pose generation, also known as pose estimation, existing approaches are typically divided into optimization-based and regression-based methods. Optimization-based methods [6, 36] estimate 3D pose parameters by aligning projected joints with detected 2D keypoints through iterative refinement. In contrast, regression-based approaches [22, 7, 12, 16] rely on deep neural networks to directly predict 3D poses from input images. Text-to-pose generation aims to synthesize 3D human poses based on textual descriptions, such as physical attributes or actions [10, 44, 18]. Although these methods have shown promising results, they remain confined to either image-to-pose or text-to-pose

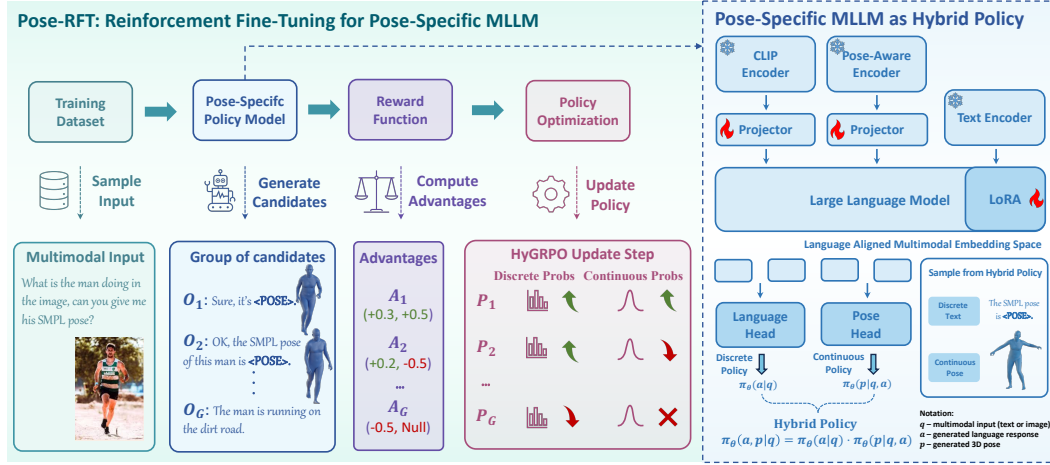


Figure 2: **Overview of Pose-RFT Framework.** A Reinforcement fine-tuning pipeline for pose-specific MLLMs. Given a multimodal input, the model generates multiple hybrid responses combining discrete text and continuous 3D pose outputs. Rewards are computed using task-specific metrics, normalized within each group, and used to update the model by promoting high-reward responses. generation, without a unified framework capable of leveraging cross-modal knowledge to infer human poses from both visual and textual inputs.

## 2.2 Multimodal Large Language Models

Multimodal Large Language Models (MLLMs) [1, 30, 24, 48, 9] have shown strong performance in vision-language understanding tasks by jointly modeling visual inputs and natural language. These models excel at multimodal reasoning, visual grounding, and instruction following, enabling them to comprehend complex visual content in diverse application scenarios. Leveraging these capabilities, recent works have successfully applied MLLMs to downstream vision-centric tasks such as image segmentation [23, 4], anomaly detection [17], and keypoint localization [47], demonstrating their transferability beyond purely linguistic domains.

To adapt MLLMs to downstream tasks, post-training strategies such as supervised fine-tuning (SFT) and reinforcement fine-tuning (RFT) are commonly used. Recent efforts such as ChatPose [14] and UniPose [27] have applied SFT to extend MLLMs for 3D pose generation, leveraging their vision-language reasoning capabilities. However, these methods rely solely on SFT and do not incorporate reinforcement-based optimization. The absence of RFT limits the model’s capacity to further refine generation quality, particularly in scenarios involving ambiguity and task-specific alignment.

## 2.3 Reinforcement Learning

Reinforcement learning (RL) [43] is a core paradigm in machine learning, where an agent learns a policy—a mapping from observations to actions—by interacting with an environment and optimizing cumulative rewards. Through trial-and-error learning, the agent improves its policy based on feedback in the form of scalar rewards. Classical algorithms such as Q-learning [50] have been successfully applied in fields such as robotics, autonomous control, and game playing. With the rise of large language models [38, 45, 1], Reinforcement Learning with Human Feedback (RLHF) [3] has become a key technique for fine-tuning models using human preference data. RLHF leverages algorithms like Proximal Policy Optimization (PPO) [40] and Direct Preference Optimization (DPO) [39] to guide model behavior for improving the alignment, coherence, and helpfulness in response generation.

In the context of multimodal large language models, recent works [56, 31, 53, 32, 52, 55, 42] have explored the use of RL with verifiable reward signals to enhance visual reasoning. However, the application of RL to 3D human pose generation remains underexplored, primarily due to the continuous nature of pose regression, which poses challenges for RL methods originally designed for discrete action spaces. To address similar challenges in other domains, several works have proposed hybrid discrete-continuous action formulations [34, 13, 25], offering a promising direction for adapting reinforcement learning to structured continuous tasks such as 3D pose generation.

### 3 Methodology

This section first reformulates 3D human pose generation as a reinforcement learning problem under a hybrid action space. It then introduces the proposed *Hybrid Action Space Group Relative Policy Optimization* (HyGRPO) algorithm, which jointly optimizes discrete language and continuous pose outputs. Finally, it describes how HyGRPO is applied to fine-tune pose-specific MLLMs using task-specific reward functions designed for 3D human pose generation.

#### 3.1 Reformulating 3D Pose Generation for Reinforcement Learning

We formulate the 3D human pose generation within pose-specific MLLMs as a hybrid action reinforcement learning problem. The model operates in a hybrid action space comprising discrete language tokens and continuous 3D poses. The overall policy is defined as:

$$\pi_\theta(a, p|q) = \pi_\theta(a|q) \cdot \pi_\theta(p|q, a), \quad (1)$$

where  $q$  denotes a multimodal input,  $a$  represents discrete textual responses, and  $p$  denotes continuous 3D pose parameters. We regard the joint distribution  $\pi_\theta(a, p|q)$  as the overall policy, which is factorized into a discrete sub-policy  $\pi_\theta(a|q)$  modeling the distribution over textual responses, and a continuous sub-policy  $\pi_\theta(p|q, a)$  modeling the distribution over 3D poses conditioned on both the input query and the generated language response.

To parameterize the continuous policy, we adopt a multivariate Gaussian distribution defined over the space of 3D human poses:

$$\pi_\theta(p|q, a) = \mathcal{N}(p; \mu_\theta(q, a), \Sigma_\theta(q, a)), \quad (2)$$

where the mean  $\mu_\theta(q, a)$  and covariance  $\Sigma_\theta(q, a)$  are predicted by a continuous pose head conditioned on the multimodal input  $q$  and the discrete response  $a$ . This probabilistic formulation captures the aleatoric uncertainty inherent in 3D human pose generation by modeling the conditional distribution over continuous pose vectors. Furthermore, the use of a differentiable multivariate Gaussian enables both stochastic sampling during training and efficient gradient-based optimization within the continuous pose space.

Benefiting from the strong cross-modal alignment established during MLLM pretraining, both the discrete and continuous policies are built on a shared language-aligned multimodal embedding space. To further enhance pose understanding, we augment the original pose-specific MLLM with a pose-aware encoder module that enriches the multimodal state representation. Specifically, we incorporate a pose-specific Vision Transformer pretrained on human pose estimation tasks to extract high-resolution, pose-sensitive features. These features are fused with the language-aligned multimodal embeddings to yield a more informative and pose-relevant state space for reinforcement learning. Details of the pose-aware encoder and the visual fusion strategy are provided in Appendix A. During optimization, each policy head is updated using its corresponding reward signal, while the shared backbone receives combined gradients, enabling end-to-end training across both discrete and continuous action spaces.

#### 3.2 HyGRPO: Hybrid Action Space Group Relative Policy Optimization

We propose Hybrid Action Space Group Relative Policy Optimization (HyGRPO), an online reinforcement learning algorithm designed to enhance pose-specific MLLMs for 3D human pose generation. Leveraging the unified representation space learned during pretraining, HyGRPO directly optimizes both the discrete language head and continuous pose head within the shared language-aligned multimodal embedding space, facilitating coherent alignment between textual and pose outputs. This algorithm effectively bridges the gap between discrete token prediction and continuous pose generation.

To handle hybrid outputs, HyGRPO models the policy  $\pi_\theta$  over both discrete text answers  $a$  and continuous human poses  $p$  conditioned on input question  $q$ . For each training sample  $q$  from dataset  $\mathcal{D}$ , we sample  $G$  output candidates  $\{a_i, p_i\}_{i=1}^G \sim \pi_\theta(\cdot|q)$ , and optimize the policy using the following objective:

$$\mathbb{E}_{q \sim \mathcal{D}, \{a_i, p_i\}_{i=1}^G \sim \pi_\theta(\cdot|q)} \left[ \frac{1}{G} \sum_{i=1}^G r_i(\theta) \hat{A}_i \right], \quad (3)$$

where  $r_i(\theta)$  is the importance weight of the  $i$ -th sampled output, computed as the ratio between the current policy and the reference policy:

$$r_i(\theta) = \frac{\pi_\theta(a_i, p_i | q)}{\pi_{\text{ref}}(a_i, p_i | q)} = \underbrace{\frac{\pi_\theta(a_i | q)}{\pi_{\text{ref}}(a_i | q)}}_{r_d(a_i | q)} \cdot \underbrace{\frac{\pi_\theta(p_i | q, a_i)}{\pi_{\text{ref}}(p_i | q, a_i)}}_{r_c(p_i | q, a_i)}. \quad (4)$$

We decompose the normalized advantage  $\hat{A}$  into two components corresponding to the discrete and continuous actions:

$$\hat{A}(q, a, p) = \underbrace{\hat{F}(q, a)}_{\text{discrete advantages}} + \underbrace{\hat{\Delta}(q, a, p)}_{\text{continuous advantages}}, \quad (5)$$

where  $\hat{F}$  measures the quality of the generated textual response, and  $\hat{\Delta}$  evaluates the predicted pose quality. To stabilize training, we adopt clipped importance sampling as in PPO [40]. The final HyGRPO training objective is:

$$\begin{aligned} \mathcal{J}_{\text{HyGRPO}} = & \mathbb{E}_{q \sim \mathcal{D}, \{a_i, p_i\}_{i=1}^G \sim \pi_\theta(\cdot | q)} \left[ \frac{1}{G} \sum_{i=1}^G \left( \min(r_d \hat{F}_i, \text{clip}(r_d, 1-\epsilon, 1+\epsilon) \hat{F}_i) \right) \right. \\ & \left. + \frac{1}{V} \sum_{i=1}^V \left( \min(r_c \hat{\Delta}_i, \text{clip}(r_c, 1-\epsilon, 1+\epsilon) \hat{\Delta}_i) \right) - \beta D_{\text{KL}}(\pi_\theta \| \pi_{\text{ref}}) \right], \end{aligned} \quad (6)$$

where  $G$  is generated candidate group,  $V$  is the candidate with pose output. This objective provides separate advantage signals for the discrete and continuous heads, while updating the shared backbone with combined gradients—enabling stable and generalizable training across the hybrid action space (see derivation in Appendix B).

Algorithm 1 describes the pseudo-code of HyGRPO. At each iteration, we sample a mini-batch of questions, generate multiple candidate outputs from the current policy, compute both types of rewards using task-specific reward models, and update the policy using the HyGRPO objective.

---

#### Algorithm 1 Hybrid Action Space Group Relative Policy Optimization

---

**Input:** Initial policy model  $\pi_{\text{init}}$  (a pretrained pose-specific MLLM); reward models  $R_\varphi$ ; task dataset  $\mathcal{D}$ ; hyperparameters  $\epsilon$

```

Initialize  $\pi_\theta \leftarrow \pi_{\text{init}}$ ,  $\pi_{\text{ref}} \leftarrow \pi_{\text{init}}$ 
for iteration = 1, ...,  $N$  do
  Sample a batch  $\mathcal{D}_b$  from  $\mathcal{D}$ 
  Generate  $G$  outputs  $\{a_i, p_i\}_{i=1}^G \sim \pi_\theta(\cdot | q)$  for each question  $q \in \mathcal{D}_b$ 
  Compute rewards  $\{\mathcal{R}_i\}_{i=1}^G$  for each  $(a_i, p_i)$  by running  $R_\varphi$ 
  Compute  $\hat{A}_i$  for  $(a_i, p_i)$  via group relative advantage estimation
  Update  $\pi_\theta$  by maximizing HyGRPO objective Eq. 6
Output: policy model  $\pi_\theta$ 

```

---

### 3.3 Enhance Pose-Specific MLLM with HyGRPO

We apply HyGRPO to optimize pose-specific MLLMs over hybrid action outputs using task-specific reward signals. As illustrated in Fig. 2, for each question  $q \in \mathcal{D}_b$ , the policy model  $\pi_\theta$  generates a group of  $G$  hybrid outputs, each consisting of a discrete textual answer and a continuous 3D pose, i.e.,  $\{O_i\}_{i=1}^G$ . For each candidate, we compute task-specific rewards that are carefully designed for different pose generation settings to guide policy updates through HyGRPO.

**Joint Location Reward in Image-to-Pose Generation.** In the image-to-pose generation task, the model is expected to output SMPL pose coefficients conditioned on the input image. To encourage spatial accuracy, the reward should reflect how well the predicted pose aligns with the visual input. A widely adopted metric in 3D human pose estimation is the mean joint position error, which computes the average Euclidean distance between predicted and ground-truth 3D joint locations. Following

this, we define the reward as the inverse of the joint error, assigning higher scores to more accurate spatial alignment:

$$\mathcal{R}_{\text{joint}} = \frac{1}{\|J_{\text{pred}} - J_{\text{gt}}\|_2}. \quad (7)$$

**Semantic Alignment Reward in Text-to-Pose Generation.** In the text-to-pose generation task, the model is expected to predict SMPL pose coefficients conditioned on a text prompt. Unlike image-to-pose generation, which emphasizes joint-level accuracy, this task focuses on high-level semantic alignment between the textual description and the generated pose.

To quantify this alignment, we adopt a pretrained text-pose retrieval model that maps both inputs into a shared embedding space. Specifically, the retrieval model comprises a text encoder  $\phi_t(\cdot)$  and a pose encoder  $\phi_p(\cdot)$ , both projecting their respective inputs into a shared embedding space. The semantic alignment reward is defined as the similarity score between the encoded text and the generated pose:

$$\mathcal{R}_{\text{semantic}} = \cos(\phi_t(q), \phi_p(p)). \quad (8)$$

**Format Reward.** To encourage the model to generate responses that conform to a specified format, we introduce a format reward, denoted as  $R_{\text{format}}$ . For instance, we expect the model to produce outputs enclosed in a template such as: “*The SMPL pose of this person is <POSE>.*” To enforce this constraint, we apply regular expression matching to assess format compliance. The format reward is defined as:

$$\mathcal{R}_{\text{format}} = \begin{cases} 1, & \text{if the output matches the expected format} \\ 0, & \text{otherwise} \end{cases}. \quad (9)$$

**Text Embedding Similarity Reward.** To preserve general QA capabilities while fine-tuning for pose-centric tasks, we incorporate a text reward that encourages semantic agreement between generated and ground-truth answers in vision-language QA tasks. Specifically, we utilize the BGE-M3 encoder [8] to compute dense embeddings for both the model-generated answer and the ground-truth response. The reward is defined as the cosine similarity between the normalized embeddings of the predicted and ground-truth answers:

$$\mathcal{R}_{\text{text}} = \cos(E(a_{\text{pred}}), E(a_{\text{gt}})). \quad (10)$$

## 4 Experiments

### 4.1 Experimental Setup

**Datasets.** To train Pose-RFT, we incorporate four types of data sources to enhance multimodal understanding: **(1) Text-Pose Data.** We utilize the PoseScript dataset [10], which provides natural language descriptions paired with 3D human poses. This enables the model to learn fine-grained semantic correlations between language and human poses. **(2) Image-Pose Data.** Following prior works [16, 14, 27], we adopt standard human pose estimation training datasets, including Human3.6M [20], MPI-INF-3DHP [35], COCO [29], and MPIII [2]. For evaluation, we use the 3DPW [46] and Human3.6M test sets. **(3) Image-Text Data.** We employ the BEDLAM-Script dataset introduced in PoseEmbroider [11], a curated multimodal dataset containing images, 3D poses, and textual descriptions, constructed based on the BEDLAM dataset [5]. **(4) VQA Data.** For visual question answering, we utilize the LLaVA-Instruct-150k dataset [30].

**Metrics.** We evaluate our model on both image-to-pose and text-to-pose tasks using reconstruction and retrieval metrics. **Image-to-Pose Reconstruction Metrics:** We report the Mean Per Joint Position Error (MPJPE) and the Procrustes-aligned MPJPE (PA-MPJPE), which measure the average Euclidean distance between predicted and ground-truth joint positions, with and without Procrustes alignment, respectively. **Text-to-Pose Retrieval Metrics:** Following [14, 27], we report Recall@K (K = 5, 10, 20) for both text-to-pose ( $R^{T2P}$ ) and pose-to-text ( $R^{P2T}$ ) retrieval tasks, which assess the accuracy of matching poses with their corresponding textual descriptions.

Table 1: **Comparison on Human Pose Estimation task.** Reconstruction metrics are reported on the 3DPW and Human3.6M datasets.

Method	3DPW [46]		Human3.6M [20]	
	MPJPE ↓	PA-MPJPE ↓	MPJPE ↓	PA-MPJPE ↓
HMR [46]	130.0	76.7	88.0	56.8
PyMAF [54]	92.8	58.9	57.7	40.5
SMPLer [51]	73.7	43.4	45.2	<b>32.4</b>
HMR2.0 [16]	70.0	44.5	<b>44.8</b>	33.6
Zolly [49]	76.2	47.9	49.4	32.3
MEGA [15]	<b>67.5</b>	<b>41.0</b>	-	-
TokenHMR [12]	71.0	44.3	-	-
ChatPose [14]	163.6	81.9	126.0	82.4
UniPose [27]	94.7	59.1	69.2	<b>41.8</b>
Pose-RFT (Ours)	<b>85.9</b>	<b>51.6</b>	<b>63.0</b>	44.5

Table 2: **Comparison on Text-to-Pose Generation Task.** Retrieval metrics (Recall@K, K=5, 10, 20) are reported on the PoseScript dataset under two evaluation protocols.

Method	PoseScript (Full Retrieval)						PoseScript (Random Sampling)					
	R <sup>T2P</sup> ↑			R <sup>P2T</sup> ↑			R <sup>T2P</sup> ↑			R <sup>P2T</sup> ↑		
PoseScript [10]	40.4	52.3	65.0	41.4	54.1	65.9	73.3	82.5	89.4	70.0	82.5	87.4
ChatPose [14]	17.6	25.3	35.8	28.0	39.0	54.4	39.9	50.6	58.7	56.1	65.3	72.5
ChatHuman [28]	41.8	52.6	65.1	42.1	52.3	66.5	-	-	-	-	-	-
UniPose [27]	-	-	-	-	-	-	<b>73.7</b>	82.4	<b>89.6</b>	70.9	80.5	89.6
Pose-RFT (Ours)	<b>42.2</b>	<b>53.0</b>	<b>65.5</b>	<b>45.3</b>	<b>57.2</b>	<b>70.4</b>	71.8	<b>82.6</b>	88.7	<b>74.6</b>	<b>86.5</b>	<b>91.5</b>

**Implementation Details.** We adopt LLaVA-1.5V-7B [30] as the vision-language backbone. For the pose-aware encoder, we employ the pretrained Vision Transformer from [16]. Reinforcement fine-tuning follows the settings of Visual-RFT [32] and VLM-R1 [42]. During both pretraining and fine-tuning, the CLIP encoder and the pose-aware encoder are kept frozen, while the projector and task head are updated. The large language model is fine-tuned using LoRA [19]. Further implementation details are provided in the Appendix C.

## 4.2 Comparisons on Human Pose Generation Tasks

**Image-to-Pose Generation.** For the image-to-pose generation task, we compare Pose-RFT with traditional pose estimation approaches [46, 54, 51, 16, 49, 15, 12] and MLLM-based approaches [14, 27], on 3DPW [46] and Human3.6M [20] datasets. As shown in Table 1, Pose-RFT significantly outperforms other pose-specific MLLMs, narrowing the performance gap between general-purpose MLLMs and task-specific pose estimation models. We attribute this improvement primarily to the pose-aware encoder, which captures more comprehensive pose-relevant information and effectively enhances the model’s ability to understand and generate human poses.

**Text-to-Pose Generation.** For the text-to-pose generation task, we compare Pose-RFT with existing text-conditional pose generation models [10, 14, 28, 27] on PoseScript-H2 test set [10], which contains 1234 high-quality human-written text-pose pairs. Since these generation models do not natively support retrieval, following previous works, we generate 3D poses from the input captions and then evaluate the results using a pretrained text-to-pose retrieval model provided by [10], computing Recall@K scores as a proxy for generation quality. As shown in Table 2, Pose-RFT achieves the best performance across most metrics. We attribute this primarily to the reinforcement fine-tuning with a semantic alignment reward, which effectively enhances the model’s ability to capture fine-grained text-pose correspondence and improves generation quality.

While prior work on text-to-pose generation is limited, existing methods evaluated their performance on the PoseScript-H2 benchmark using two different retrieval protocols. To ensure fair and comprehensive comparison, we report results under both protocols: **Protocol 1 (Full Retrieval)** follows the standard one-to-one retrieval setting, where each query corresponds to a single target in the entire test

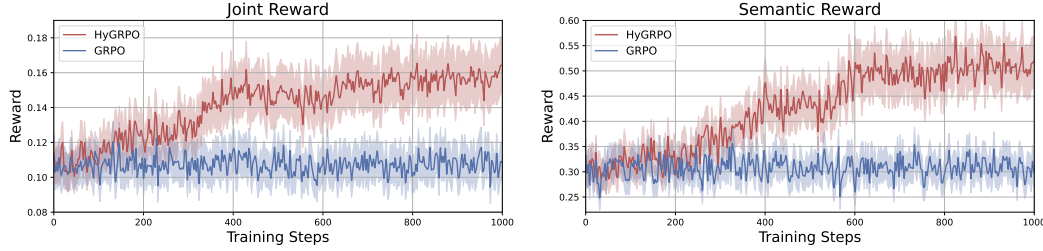


Figure 3: **Comparison between GRPO and HyGRPO.** The horizontal axis represents the number of training steps. The vertical axis shows the mean group reward, computed across sampled candidate poses for each input.

set. We compute Recall@K over the full test set, where each query is matched to its corresponding ground-truth pose based on dataset pairing. **Protocol 2 (Random Sampling)**, in contrast, adopts the commonly used Recall@K evaluation under random sampling. For each query, we randomly sample  $N = 32$  candidates (including the ground-truth), and repeat the retrieval process  $R = 10$  times to average out the variance.

### 4.3 Ablation Studies and Discussions

**Pose-Aware Encoder.** We evaluate the effectiveness of the proposed pose-aware encoder across the full training process. As shown in Fig. 4, the pose-aware model achieves a higher joint location reward score on the 3DPW dataset compared to the baseline model. This result indicates that relying solely on a CLIP encoder is suboptimal for pose estimation tasks. In contrast, by incorporating an additional Vision Transformer pretrained on pose estimation and adopting a token-level feature fusion strategy, the pose-aware model captures fine-grained pose information more effectively, leading to significant improvements in pose accuracy. However, we observe that the pose-aware encoder brings little benefit to the text-to-pose semantic reward, possibly because the additional visual tokens are less aligned with the textual input, limiting their contribution to cross-modal understanding.

**GRPO vs. HyGRPO.** We compare the effectiveness of GRPO and the proposed HyGRPO algorithm for reinforcement fine-tuning of pose-specific MLLMs. In this experiment, both methods are applied to models trained on the multi-task dataset. As shown in Fig. 3, GRPO, which solely optimizes next-token prediction in the discrete action space, brings negligible improvement to the quality of 3D pose generation. In contrast, HyGRPO jointly optimizes discrete token outputs and continuous 3D pose parameters under the guidance of task-specific reward functions. Leveraging the semantic alignment and joint location reward—both of which quantitatively assess output quality—HyGRPO yields consistent improvements in reward scores during training, indicating better alignment in both text- and image-conditioned pose generation.

**Reinforcement Fine-tuning.** We evaluate the effectiveness of Pose-RFT through reinforcement fine-tuning using HyGRPO. Starting from a pretrained pose-specific MLLM, the model is fine-tuned on the multi-task dataset for 1,000 steps. As shown in Fig. 4, reinforcement fine-tuning consistently improves both text-to-pose and image-to-pose generation performance on the PoseScript and 3DPW datasets, respectively, with particularly notable gains in the text-to-pose setting. These results demonstrate the efficacy of reinforcement learning in enhancing the alignment between language, vision, and 3D pose representations. Additionally, we observe that the reward improvement on the text-to-pose task is substantially greater than that on the image-to-pose task. We attribute this to the strong joint modeling capability of the pretrained text-pose retrieval model [10], that effectively guide text-conditioned pose generation.

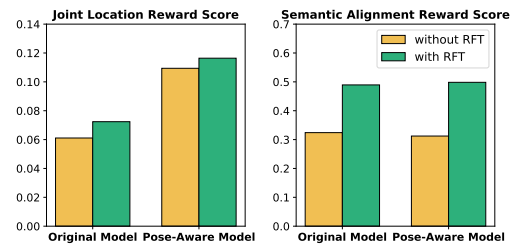


Figure 4: Ablation study of Pose-Aware Encoder (left/right bars in each group) and Reinforcement Fine-tuning (color-coded). Semantic alignment reward score are averaged over the PoseScript-H2 test set, while joint location reward scores are averaged over the 3DPW test set.

Table 3: Ablation study on distributional modeling (denoted as “Dist.”) for 3D pose generation. Reconstruction and retrieval metrics are reported on the 3DPW and PoseScript-H2 datasets.

Method	Dist.	RFT	Image-to-Pose Generation		Text-to-Pose Generation	
			MPJPE ↓	PA-MPJPE ↓	mRecall <sup>T2P</sup> ↑	mRecall <sup>P2T</sup> ↑
Baseline	✗	✗	90.4	57.1	36.2	41.5
Baseline + Dist.	✓	✗	91.4	59.2	37.4	42.0
Baseline + Dist. + RFT	✓	✓	85.9	51.6	53.6	57.6

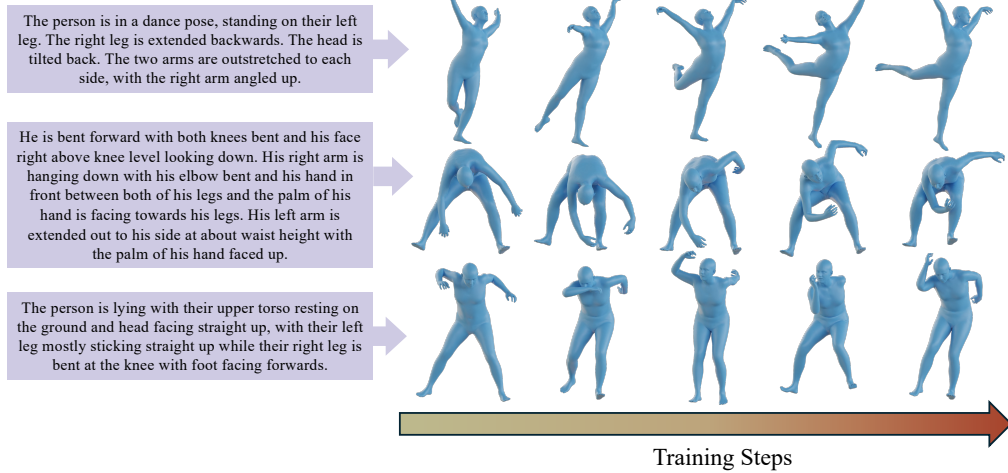


Figure 5: **Training progression of text-to-pose generation.** 3D poses sampled at different reinforcement fine-tuning steps, conditioned on the same text prompt. As reinforcement fine-tuning progresses with the semantic alignment reward, the generated poses exhibit increasingly improved semantic consistency and structural plausibility.

**Distributional Modeling in Pose Generation** To assess the impact of modeling 3D human pose generation as a probabilistic distribution, we conduct an ablation study comparing our Gaussian policy to a standard deterministic regression baseline. As shown in Table 3, without reinforcement fine-tuning, the distributional head performs slightly worse than the deterministic counterpart. However, when reinforcement signals are introduced, the probabilistic model achieves significantly better performance. These results suggest that distributional modeling facilitates more effective reward-driven learning, enabling the model to better integrate semantic and spatial feedback from multimodal inputs and produce higher-quality 3D poses.

#### 4.4 Qualitative Results

As shown in Fig. 5, we present qualitative examples of 3D poses generated from a fixed set of text prompts. For each prompt, we visualize poses sampled at different reinforcement fine-tuning steps (left to right). These results illustrate the model’s progressive improvement in generating poses that are semantically aligned with the corresponding textual descriptions.

### 5 Conclusion

In this paper, we present Pose-RFT, the first reinforcement fine-tuning framework specifically designed to enhance 3D pose generation in pose-specific MLLMs. To address the challenges of discrete-continuous hybrid action space, we introduce Hybrid Action Space Group Relative Policy Optimization (HyGRPO), a novel reinforcement learning algorithm that jointly optimizes textual responses and 3D pose outputs. By incorporating task-specific reward functions that capture both spatial accuracy and semantic alignment, Pose-RFT effectively improves generation quality under different input modalities. Extensive experiments across multiple benchmarks demonstrate that Pose-RFT consistently outperforms existing pose-specific MLLMs, validating the effectiveness of hybrid action reinforcement fine-tuning for 3D pose generation tasks.

## References

- [1] Josh Achiam, Steven Adler, Sandhini Agarwal, Lama Ahmad, Ilge Akkaya, Florencia Leoni Aleman, Diogo Almeida, Janko Altenschmidt, Sam Altman, Shyamal Anadkat, et al. Gpt-4 technical report. *arXiv preprint arXiv:2303.08774*, 2023.
- [2] Mykhaylo Andriluka, Leonid Pishchulin, Peter Gehler, and Bernt Schiele. 2d human pose estimation: New benchmark and state of the art analysis. In *Proceedings of the IEEE Conference on computer Vision and Pattern Recognition*, pages 3686–3693, 2014.
- [3] Yuntao Bai, Andy Jones, Kamal Ndousse, Amanda Askell, Anna Chen, Nova DasSarma, Dawn Drain, Stanislav Fort, Deep Ganguli, Tom Henighan, et al. Training a helpful and harmless assistant with reinforcement learning from human feedback. *arXiv preprint arXiv:2204.05862*, 2022.
- [4] Zechen Bai, Tong He, Haiyang Mei, Pichao Wang, Ziteng Gao, Joya Chen, Zheng Zhang, and Mike Zheng Shou. One token to seg them all: Language instructed reasoning segmentation in videos. *Advances in Neural Information Processing Systems*, 37:6833–6859, 2024.
- [5] Michael J Black, Priyanka Patel, Joachim Tesch, and Jinlong Yang. Bedlam: A synthetic dataset of bodies exhibiting detailed lifelike animated motion. In *Proceedings of the IEEE/CVF Conference on Computer Vision and Pattern Recognition*, pages 8726–8737, 2023.
- [6] Federica Bogo, Angjoo Kanazawa, Christoph Lassner, Peter Gehler, Javier Romero, and Michael J Black. Keep it smpl: Automatic estimation of 3d human pose and shape from a single image. In *Computer Vision–ECCV 2016: 14th European Conference, Amsterdam, The Netherlands, October 11–14, 2016, Proceedings, Part V 14*, pages 561–578. Springer, 2016.
- [7] Zhongang Cai, Wanqi Yin, Ailing Zeng, Chen Wei, Qingping Sun, Wang Yanjun, Hui En Pang, Haiyi Mei, Mingyuan Zhang, Lei Zhang, et al. Smpler-x: Scaling up expressive human pose and shape estimation. *Advances in Neural Information Processing Systems*, 36:11454–11468, 2023.
- [8] Jianlv Chen, Shitao Xiao, Peitian Zhang, Kun Luo, Defu Lian, and Zheng Liu. Bge m3-embedding: Multi-lingual, multi-functionality, multi-granularity text embeddings through self-knowledge distillation. *arXiv preprint arXiv:2402.03216*, 2024.
- [9] Zhe Chen, Jiannan Wu, Wenhui Wang, Weijie Su, Guo Chen, Sen Xing, Muyan Zhong, Qinglong Zhang, Xizhou Zhu, Lewei Lu, et al. Internvl: Scaling up vision foundation models and aligning for generic visual-linguistic tasks. In *Proceedings of the IEEE/CVF conference on computer vision and pattern recognition*, pages 24185–24198, 2024.
- [10] Ginger Delmas, Philippe Weinzaepfel, Thomas Lucas, Francesc Moreno-Noguer, and Grégory Rogez. Posescript: 3d human poses from natural language. In *European Conference on Computer Vision*, pages 346–362. Springer, 2022.
- [11] Ginger Delmas, Philippe Weinzaepfel, Francesc Moreno-Noguer, and Grégory Rogez. Poseembroider: Towards a 3d, visual, semantic-aware human pose representation. In *European Conference on Computer Vision*, pages 55–73. Springer, 2024.
- [12] Sai Kumar Dwivedi, Yu Sun, Priyanka Patel, Yao Feng, and Michael J Black. Tokenhmr: Advancing human mesh recovery with a tokenized pose representation. In *Proceedings of the IEEE/CVF Conference on Computer Vision and Pattern Recognition*, pages 1323–1333, 2024.
- [13] Zhou Fan, Rui Su, Weinan Zhang, and Yong Yu. Hybrid actor-critic reinforcement learning in parameterized action space. *arXiv preprint arXiv:1903.01344*, 2019.
- [14] Yao Feng, Jing Lin, Sai Kumar Dwivedi, Yu Sun, Priyanka Patel, and Michael J Black. Chatpose: Chatting about 3d human pose. In *Proceedings of the IEEE/CVF conference on computer vision and pattern recognition*, pages 2093–2103, 2024.
- [15] Guénolé Fiche, Simon Leglaive, Xavier Alameda-Pineda, and Francesc Moreno-Noguer. Mega: Masked generative autoencoder for human mesh recovery. *arXiv preprint arXiv:2405.18839*, 2024.

[16] Shubham Goel, Georgios Pavlakos, Jathushan Rajasegaran, Angjoo Kanazawa, and Jitendra Malik. Humans in 4d: Reconstructing and tracking humans with transformers. In *Proceedings of the IEEE/CVF International Conference on Computer Vision*, pages 14783–14794, 2023.

[17] Zhaopeng Gu, Bingke Zhu, Guibo Zhu, Yingying Chen, Ming Tang, and Jinqiao Wang. Anomalygpt: Detecting industrial anomalies using large vision-language models. In *Proceedings of the AAAI conference on artificial intelligence*, volume 38, pages 1932–1940, 2024.

[18] Fangzhou Hong, Mingyuan Zhang, Liang Pan, Zhongang Cai, Lei Yang, and Ziwei Liu. Avatarclip: Zero-shot text-driven generation and animation of 3d avatars. *arXiv preprint arXiv:2205.08535*, 2022.

[19] Edward J Hu, Yelong Shen, Phillip Wallis, Zeyuan Allen-Zhu, Yuanzhi Li, Shean Wang, Lu Wang, Weizhu Chen, et al. Lora: Low-rank adaptation of large language models. *ICLR*, 1(2):3, 2022.

[20] Catalin Ionescu, Dragos Papava, Vlad Olaru, and Cristian Sminchisescu. Human3. 6m: Large scale datasets and predictive methods for 3d human sensing in natural environments. *IEEE transactions on pattern analysis and machine intelligence*, 36(7):1325–1339, 2013.

[21] Aaron Jaech, Adam Kalai, Adam Lerer, Adam Richardson, Ahmed El-Kishky, Aiden Low, Alec Helyar, Aleksander Madry, Alex Beutel, Alex Carney, et al. Openai o1 system card. *arXiv preprint arXiv:2412.16720*, 2024.

[22] Angjoo Kanazawa, Michael J. Black, David W. Jacobs, and Jitendra Malik. End-to-end recovery of human shape and pose. In *Computer Vision and Pattern Recognition (CVPR)*, 2018.

[23] Xin Lai, Zhuotao Tian, Yukang Chen, Yanwei Li, Yuhui Yuan, Shu Liu, and Jiaya Jia. Lisa: Reasoning segmentation via large language model. In *Proceedings of the IEEE/CVF Conference on Computer Vision and Pattern Recognition*, pages 9579–9589, 2024.

[24] Bo Li, Yuanhan Zhang, Dong Guo, Renrui Zhang, Feng Li, Hao Zhang, Kaichen Zhang, Peiyuan Zhang, Yanwei Li, Ziwei Liu, et al. Llava-onevision: Easy visual task transfer. *arXiv preprint arXiv:2408.03326*, 2024.

[25] Boyan Li, Hongyao Tang, Yan Zheng, Jianye Hao, Pengyi Li, Zhen Wang, Zhaopeng Meng, and Li Wang. Hyar: Addressing discrete-continuous action reinforcement learning via hybrid action representation. *arXiv preprint arXiv:2109.05490*, 2021.

[26] Xinhao Li, Ziang Yan, Desen Meng, Lu Dong, Xiangyu Zeng, Yinan He, Yali Wang, Yu Qiao, Yi Wang, and Limin Wang. Videochat-r1: Enhancing spatio-temporal perception via reinforcement fine-tuning. *arXiv preprint arXiv:2504.06958*, 2025.

[27] Yiheng Li, Ruibing Hou, Hong Chang, Shiguang Shan, and Xilin Chen. Unipose: A unified multimodal framework for human pose comprehension, generation and editing. *arXiv preprint arXiv:2411.16781*, 2024.

[28] Jing Lin, Yao Feng, Weiyang Liu, and Michael J Black. Chathuman: Language-driven 3d human understanding with retrieval-augmented tool reasoning. *arXiv preprint arXiv:2405.04533*, 2024.

[29] Tsung-Yi Lin, Michael Maire, Serge Belongie, James Hays, Pietro Perona, Deva Ramanan, Piotr Dollár, and C Lawrence Zitnick. Microsoft coco: Common objects in context. In *Computer vision–ECCV 2014: 13th European conference, zurich, Switzerland, September 6–12, 2014, proceedings, part v 13*, pages 740–755. Springer, 2014.

[30] Haotian Liu, Chunyuan Li, Qingyang Wu, and Yong Jae Lee. Visual instruction tuning. *Advances in neural information processing systems*, 36:34892–34916, 2023.

[31] Yuqi Liu, Bohao Peng, Zhisheng Zhong, Zihao Yue, Fanbin Lu, Bei Yu, and Jiaya Jia. Seg-zero: Reasoning-chain guided segmentation via cognitive reinforcement. *arXiv preprint arXiv:2503.06520*, 2025.

[32] Ziyu Liu, Zeyi Sun, Yuhang Zang, Xiaoyi Dong, Yuhang Cao, Haodong Duan, Dahua Lin, and Jiaqi Wang. Visual-rft: Visual reinforcement fine-tuning. *arXiv preprint arXiv:2503.01785*, 2025.

[33] Matthew Loper, Naureen Mahmood, Javier Romero, Gerard Pons-Moll, and Michael J Black. Smpl: A skinned multi-person linear model. In *Seminal Graphics Papers: Pushing the Boundaries, Volume 2*, pages 851–866. 2023.

[34] Ryan Lowe, Yi I Wu, Aviv Tamar, Jean Harb, OpenAI Pieter Abbeel, and Igor Mordatch. Multi-agent actor-critic for mixed cooperative-competitive environments. *Advances in neural information processing systems*, 30, 2017.

[35] Dushyant Mehta, Helge Rhodin, Dan Casas, Pascal Fua, Oleksandr Sotnychenko, Weipeng Xu, and Christian Theobalt. Monocular 3d human pose estimation in the wild using improved cnn supervision. In *2017 international conference on 3D vision (3DV)*, pages 506–516. IEEE, 2017.

[36] Georgios Pavlakos, Vasileios Choutas, Nima Ghorbani, Timo Bolkart, Ahmed AA Osman, Dimitrios Tzionas, and Michael J Black. Expressive body capture: 3d hands, face, and body from a single image. In *Proceedings of the IEEE/CVF conference on computer vision and pattern recognition*, pages 10975–10985, 2019.

[37] Alec Radford, Jong Wook Kim, Chris Hallacy, Aditya Ramesh, Gabriel Goh, Sandhini Agarwal, Girish Sastry, Amanda Askell, Pamela Mishkin, Jack Clark, et al. Learning transferable visual models from natural language supervision. In *International conference on machine learning*, pages 8748–8763. PMLR, 2021.

[38] Alec Radford, Karthik Narasimhan, Tim Salimans, Ilya Sutskever, et al. Improving language understanding by generative pre-training.(2018), 2018.

[39] Rafael Rafailov, Archit Sharma, Eric Mitchell, Christopher D Manning, Stefano Ermon, and Chelsea Finn. Direct preference optimization: Your language model is secretly a reward model. *Advances in Neural Information Processing Systems*, 36:53728–53741, 2023.

[40] John Schulman, Filip Wolski, Prafulla Dhariwal, Alec Radford, and Oleg Klimov. Proximal policy optimization algorithms. *arXiv preprint arXiv:1707.06347*, 2017.

[41] Zhihong Shao, Peiyi Wang, Qihao Zhu, Runxin Xu, Junxiao Song, Xiao Bi, Haowei Zhang, Mingchuan Zhang, YK Li, Y Wu, et al. Deepseekmath: Pushing the limits of mathematical reasoning in open language models. *arXiv preprint arXiv:2402.03300*, 2024.

[42] Haozhan Shen, Peng Liu, Jingcheng Li, Chunxin Fang, Yibo Ma, Jiajia Liao, Qiaoli Shen, Zilun Zhang, Kangjia Zhao, Qianqian Zhang, et al. Vlm-r1: A stable and generalizable r1-style large vision-language model. *arXiv preprint arXiv:2504.07615*, 2025.

[43] Richard S Sutton, Andrew G Barto, et al. *Reinforcement learning: An introduction*, volume 1. MIT press Cambridge, 1998.

[44] Guy Tevet, Sigal Raab, Brian Gordon, Yonatan Shafir, Daniel Cohen-Or, and Amit H Bermano. Human motion diffusion model. *arXiv preprint arXiv:2209.14916*, 2022.

[45] Hugo Touvron, Thibaut Lavril, Gautier Izacard, Xavier Martinet, Marie-Anne Lachaux, Timothée Lacroix, Baptiste Rozière, Naman Goyal, Eric Hambro, Faisal Azhar, et al. Llama: Open and efficient foundation language models. *arXiv preprint arXiv:2302.13971*, 2023.

[46] Timo Von Marcard, Roberto Henschel, Michael J Black, Bodo Rosenhahn, and Gerard Pons-Moll. Recovering accurate 3d human pose in the wild using imus and a moving camera. In *Proceedings of the European conference on computer vision (ECCV)*, pages 601–617, 2018.

[47] Dongkai Wang, Shiyu Xuan, and Shiliang Zhang. Locllm: Exploiting generalizable human keypoint localization via large language model. In *Proceedings of the IEEE/CVF conference on computer vision and pattern recognition*, pages 614–623, 2024.

[48] Peng Wang, Shuai Bai, Sinan Tan, Shijie Wang, Zhihao Fan, Jinze Bai, Keqin Chen, Xuejing Liu, Jialin Wang, Wenbin Ge, et al. Qwen2-vl: Enhancing vision-language model’s perception of the world at any resolution. *arXiv preprint arXiv:2409.12191*, 2024.

[49] Wenjia Wang, Yongtao Ge, Haiyi Mei, Zhongang Cai, Qingping Sun, Yanjun Wang, Chunhua Shen, Lei Yang, and Taku Komura. Zolly: Zoom focal length correctly for perspective-distorted human mesh reconstruction. In *Proceedings of the IEEE/CVF international conference on computer vision*, pages 3925–3935, 2023.

[50] Christopher JCH Watkins and Peter Dayan. Q-learning. *Machine learning*, 8:279–292, 1992.

[51] Xiangyu Xu, Lijuan Liu, and Shuicheng Yan. Smpler: Taming transformers for monocular 3d human shape and pose estimation. *IEEE Transactions on Pattern Analysis and Machine Intelligence*, 46(5):3275–3289, 2023.

[52] Yi Yang, Xiaoxuan He, Hongkun Pan, Xiyan Jiang, Yan Deng, Xingtao Yang, Haoyu Lu, Dacheng Yin, Fengyun Rao, Minfeng Zhu, et al. R1-onevision: Advancing generalized multimodal reasoning through cross-modal formalization. *arXiv preprint arXiv:2503.10615*, 2025.

[53] Yufei Zhan, Yousong Zhu, Shurong Zheng, Hongyin Zhao, Fan Yang, Ming Tang, and Jinqiao Wang. Vision-r1: Evolving human-free alignment in large vision-language models via vision-guided reinforcement learning. *arXiv preprint arXiv:2503.18013*, 2025.

[54] Hongwen Zhang, Yating Tian, Xinchi Zhou, Wanli Ouyang, Yebin Liu, Limin Wang, and Zhenan Sun. Pymaf: 3d human pose and shape regression with pyramidal mesh alignment feedback loop. In *Proceedings of the IEEE/CVF international conference on computer vision*, pages 11446–11456, 2021.

[55] Jingyi Zhang, Jiaxing Huang, Huanjin Yao, Shunyu Liu, Xikun Zhang, Shijian Lu, and Dacheng Tao. R1-vl: Learning to reason with multimodal large language models via step-wise group relative policy optimization. *arXiv preprint arXiv:2503.12937*, 2025.

[56] Hengguang Zhou, Xirui Li, Ruochen Wang, Minhao Cheng, Tianyi Zhou, and Cho-Jui Hsieh. R1-zero's" aha moment" in visual reasoning on a 2b non-sft model. *arXiv preprint arXiv:2503.05132*, 2025.

## A Details of Pose-Aware Encoder and the Visual Fusion Strategy

This section provides additional implementation details of the Pose-Aware Encoder and the corresponding visual feature fusion strategy used in our framework.

Previous works [30, 14] typically adopt the CLIP visual encoder [37] as the visual backbone. However, since CLIP is pretrained using global and coarse-grained supervision from image-caption pairs, it struggles to capture fine-grained pose details. In contrast, pose estimation tasks require precise localization of human keypoints, encouraging the encoder to learn fine-grained, pose-aware representations. To address this limitation, we introduce a pose-specific Vision Transformer [16] pretrained on human pose estimation into the visual pipeline, as illustrated in Fig. 1.

Let  $f_a$  denote the CLIP visual encoder and  $f_b$  the pose-aware encoder. Given an input image  $x$ , we extract two sets of visual embeddings:  $v_a = f_a(x) \in \mathbb{R}^{L_v \times d_a}$  and  $v_b = f_b(x) \in \mathbb{R}^{L_v \times d_b}$ , where  $L_v$  is the number of visual tokens, and  $d_a, d_b$  are the respective embedding dimensions. While UniPose [27] directly concatenates  $v_a$  and  $v_b$  along the channel dimension and applies a single linear projection  $W \in \mathbb{R}^{(d_a+d_b) \times d}$  this design can lead to patch-level misalignment due to the differing preprocessing pipelines of the two encoders, potentially degrading performance.

To preserve the individual strengths of each visual encoder, we propose to project  $v_a$  and  $v_b$  individually using two separate linear layers:

$$v'_a = W_a v_a, \quad v'_b = W_b v_b, \quad W_a \in \mathbb{R}^{d_a \times d}, \quad W_b \in \mathbb{R}^{d_b \times d} \quad (11)$$

The transformed features  $v'_a$  and  $v'_b$  are then used in a token-level fusion with language features during joint training. This design maintains the representational integrity of both visual encoders while aligning their output with the language model's embedding space.

## B Theoretical Derivation of the HyGRPO Objective

Our goal is to optimize a hybrid policy  $\pi_\theta(a, p|q)$ , where  $a$  is a discrete action (e.g., text sequence), and  $p$  is continuous action (e.g., 3D human pose), both conditioned on the input  $q$ . We assume the policy factorizes as:

$$\pi_\theta(a, p|q) = \pi_d(a|q) \cdot \pi_c(p|q, a), \quad (12)$$

where  $\pi_d$  is the discrete policy and  $\pi_c$  is the continuous policy conditioned on the discrete output. To simplify the derivation, we temporarily exclude the clipping and KL regularization terms from the GRPO [41] objective. These components are included in the final training objective but are omitted here for clarity. We begin with the simplified form of the GRPO objective :

$$\mathbb{E}_{q \sim \mathcal{D}, \{a_i, p_i\}_{i=1}^G \sim \pi_\theta(\cdot|q)} \left[ \frac{1}{G} \sum_{i=1}^G r_i(\theta) \hat{A}_i \right]. \quad (13)$$

Here,  $r_i(\theta)$  is the importance weight of the  $i$ -th sampled output, computed as the ratio between the current policy and the reference policy:

$$r_i(\theta) = \frac{\pi_\theta(a_i, p_i|q)}{\pi_{\text{ref}}(a_i, p_i|q)} = \underbrace{\frac{\pi_\theta(a_i|q)}{\pi_{\text{ref}}(a_i|q)}}_{r_d(a_i|q)} \cdot \underbrace{\frac{\pi_\theta(p_i|q, a_i)}{\pi_{\text{ref}}(p_i|q, a_i)}}_{r_c(p_i|q, a_i)}. \quad (14)$$

To effectively train the hybrid policy, we decompose the surrogate loss into discrete and continuous components. This is motivated by the nature of our task design, where the rewards are defined separately for the discrete and continuous outputs: textual rewards  $R_d(q, a)$  evaluate the semantic correctness of the generated answer  $a$ . pose rewards  $R_c(q, a, p)$  measures the plausibility and relevance of the generated pose  $p$  conditioned on both the question and answer.

Accordingly, we decompose the advantage estimate into discrete and continuous components:

$$\hat{A}(q, a, p) = \underbrace{\hat{F}(q, a)}_{\text{discrete advantages}} + \underbrace{\hat{\Delta}(q, a, p)}_{\text{continuous advantages}}. \quad (15)$$

This decomposition does not rely on an additive assumption over a shared reward function. Instead, it reflects the fact that the discrete and continuous components are supervised by independent reward signals tailored to their modalities. Accordingly, we compute two independent advantages from these separate rewards, using per-sample normalization within the candidate set:

$$\hat{F}(q, a_i) = \frac{R_d^{(i)} - \text{mean}(\{R_d\}_{i=1}^G)}{\text{std}(\{R_d\}_{i=1}^G)} \quad \hat{\Delta}_i(q, a_i, p_i) = \frac{R_c^{(i)} - \text{mean}(\{R_c\}_{i=1}^G)}{\text{std}(\{R_c\}_{i=1}^G)}. \quad (16)$$

We now substitute this decomposition into the GRPO objective. To facilitate this, we first move the expectation over the continuous action into an inner term:

$$\mathbb{E}_{q \sim \mathcal{D}, \{a_i\}_{i=1}^G \sim \pi_\theta(\cdot|q)} \left[ \frac{1}{G} \sum_{i=1}^G r_d(a_i|q) \underbrace{\mathbb{E}_{p_i \sim \pi_\theta(p|q, a_i)} [r_c(p_i|q, a_i) \hat{A}_i(q, a_i, p_i)]}_{=: G(q, a_i)} \right], \quad (17)$$

We then analyze the inner term  $G(q, a_i)$  by substituting the advantage decomposition:

$$\begin{aligned} G(q, a_i) &= \mathbb{E}_{p_i \sim \pi_\theta(p|q, a_i)} [r_c(p_i|q, a_i) \hat{F}_i(q, a_i) + r_c(p_i|q, a_i) \hat{\Delta}_i(q, a_i, p_i)] \\ &= \hat{F}(q, a_i) \underbrace{\mathbb{E}_{p_i \sim \pi_\theta(p|q, a_i)} [r_c(q, a_i, p_i)]}_{=1} + \mathbb{E}_{p_i \sim \pi_\theta(p|q, a_i)} [r_c(q, a_i, p_i) \hat{\Delta}_i(q, a_i, p_i)] \\ &= \hat{F}_i(q, a_i) + \mathbb{E}_{p_i \sim \pi_\theta(p|q, a_i)} [r_c(q, a_i, p_i) \hat{\Delta}_i(q, a_i, p_i)]. \end{aligned} \quad (18)$$

Substituting  $G(q, a_i)$  back into the outer expectation, we arrive at a natural decomposition into two components:

$$\underbrace{\mathbb{E}_{q \sim \mathcal{D}, \{a_i\}_{i=1}^G \sim \pi_\theta(\cdot|q)} [r_d(a_i|q) \hat{F}_i(q, a_i)]}_{\mathcal{J}_d} + \underbrace{\mathbb{E}_{q \sim \mathcal{D}, \{a_i, p_i\}_{i=1}^G \sim \pi_\theta(\cdot|q)} [r_d(q, a_i) r_c(q, a_i, p_i) \hat{\Delta}_i(q, a_i, p_i)]}_{\mathcal{J}_c}. \quad (19)$$

Table 4: Hyperparameter settings of pose-specific MLLM pretraining and reinforcement fine-tuning.

Hyperparameters	Pretraining	Reinforcement fine-tuning
Batch Size	80	16
Learning Rate	3e-4	1e-6
Training Steps	10000	1000
Optimizer	AdamW	AdamW
Adam $\beta$	(0.9, 0.95)	(0.9, 0.95)
LR Schedule	Cosine	Cosine
Computing Resources	NVIDIA A100 (40GB)	NVIDIA A800 (80GB)

Although the discrete importance weight  $r_d(a|q)$  and the continuous policy  $\pi_\theta(p|q, a)$  share a common embedding space and are thus implicitly coupled through shared parameters,  $r_d(a|q)$  does not directly depend on the parameters of the continuous branch. In practice, when generating valid continuous 3D poses, the discrete answers  $q$  are highly templated. Thus,  $r_d(a|q)$  can be treated as a constant with respect to the optimization of the continuous component. Therefore, the continuous policy gradient is proportional to:

$$\nabla_\theta J_c \propto \nabla_\theta \mathbb{E}_{q \sim \mathcal{D}, \{a_i, p_i\}_{i=1}^G \sim \pi_\theta(\cdot|q)} [r_c(q, a_i, p_i) \hat{\Delta}_i(q, a_i, p_i)]. \quad (20)$$

Based on the decomposed gradient structure, we apply PPO-style [40] clipping separately to the discrete and continuous components to stabilize training:

$$\begin{aligned} \mathcal{J}_{\text{HyGRPO}} = & \mathbb{E}_{(q, a, p) \sim \mathcal{D}, \{a_i, p_i\}_{i=1}^G \sim \pi_\theta(\cdot|q)} \left[ \frac{1}{G} \sum_{i=1}^G \left( \min(r_d \hat{F}_i, \text{clip}(r_d, 1-\epsilon, 1+\epsilon) \hat{F}_i) \right) \right. \\ & \left. + \frac{1}{V} \sum_{i=1}^V \left( \min(r_c \hat{\Delta}_i, \text{clip}(r_c, 1-\epsilon, 1+\epsilon) \hat{\Delta}_i) \right) - \beta D_{\text{KL}}(\pi_\theta \| \pi_{\text{ref}}) \right]. \end{aligned} \quad (21)$$

where  $G$  is the total number of sampled candidates per input, and  $V \leq G$  is the number of candidates with valid continuous outputs. This objective enables separate, stable, and reward-aligned optimization of discrete and continuous policy branches within a unified reinforcement learning framework.

## C Experimental Details

The detailed hyperparameter settings for both Pose-specific MLLM pretraining and reinforcement fine-tuning are provided in Table 4. In the pretraining stage, we focus on adapting the base LLaVA [30] model to 3D pose tasks, while the reinforcement fine-tuning stage further optimizes the policy behavior.

## D Limitations

While our method represents a promising step toward reinforcement learning-based 3D human pose generation, it has several limitations. First, its effectiveness is inherently constrained by the quality of the reward functions. Designing reliable and semantically meaningful reward signals for pose generation remains a challenging problem, especially when capturing nuanced human preferences such as plausibility, naturalness, or contextual relevance. Inaccurate or incomplete reward feedback may misguide policy optimization, leading to suboptimal or unnatural poses.

Second, our framework relies on sampling multiple candidate responses per input to perform group-wise reward normalization. Although this design improves training stability in hybrid action spaces, it introduces non-negligible computational overhead, which may limit scalability when applied to larger models or datasets.